Highly sensitive detection for acetic acid based on biomorphic ZIF-8 and MOFs dual-template-derived ZnO-rGO nanocomposites

Haixia Chen,* Gaige Zhang, Jijun Ding, and Haiwei Fu

Shaanxi Engineering Research Center of Oil and Gas Resource Optical Fiber Detection, Shaanxi Key Laboratory of Measurement and Control Technology for Oil and Gas wells, College of Science, Xi'an Shiyou University, Xi'an, 710065, China

*Corresponding author(s). E-mail(s): chenhx@xsyu.edu.cn

Thermal bypass gas sensor is used in this work. The sensor chip is shown in Fig. S1 (a), and it consists of gas sensor base, gas sensor ceramic tube, gas sensor heating wire and sensitive material. Among them, the gas sensor base is shown in Fig. S1(b), and its specifications are 18.78 mm in diameter, 5.59 mm in thickness and 16.76 mm in wire length. Fig. S1(c) shows the gas sensor ceramic tube with the tube length of 4 mm, outer diameter of 1.2 mm, electrode spacing of 0.8-1.0 mm and uniform electrode spacing. Fig. S1(d) shows the gas sensor heating wire with a resistance value of 28-30 Ω, and the length of the two ends of the heating wire is 10-20 mm and the length of the spiral ring is about 4 mm. A static test method is used in testing the response of the target gas. The target gas is prepared by injecting a certain amount of volatile solution into the chamber using a pointed micro syringe and mixing it with the air inside the chamber. The concentration of the target gas is calculated according to the equation [1, 2].

$$C = \frac{22.4 \times \varphi \times \rho \times V_1}{M \times V_2} \times 1000$$

Where, C (ppm) is the target gas concentration, φ is the desired gas volume fraction, ρ (g/mL) is the density of the liquid, V_1 (μL) is the volume of the liquid, V_2 (L) is the volume of the chamber, and M (g/mol) is the molecular weight of the liquid. The WS-30B is connected to the PC port, and when the target gas comes into contact with the sensitive material, it will cause a change in the resistance value of the sensitive materials. The resistance value of the sensor in air and in the target gas are defined as R_a and R_g, respectively.

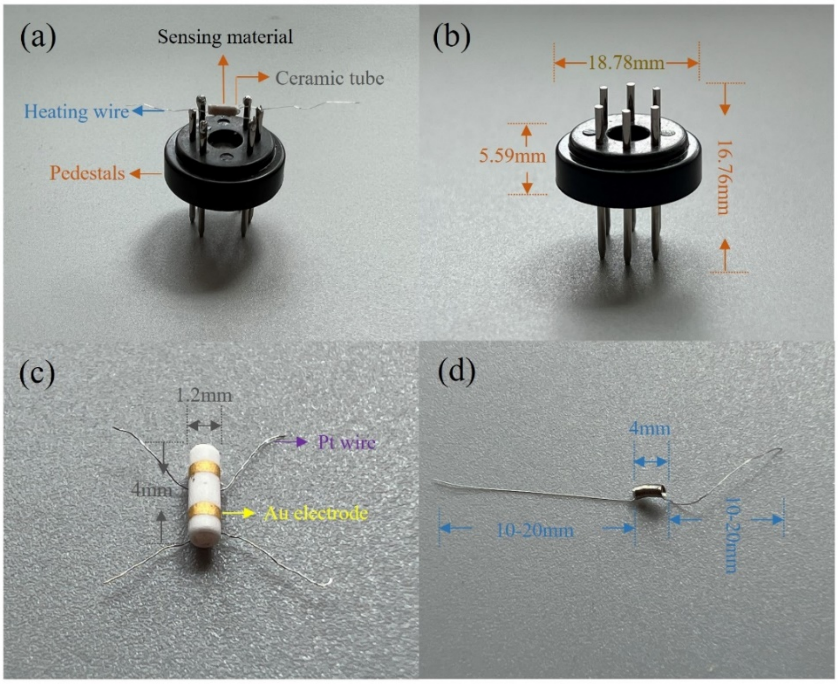

Fig. S1 (a) Thermal bypass gas sensors chip after welding, (b) Gas sensor base, (c) Gas sensor ceramic tube, and (d) Gas sensor heating wire.

Raman spectra can be used to detect chemical structure, phases, morphology, crystallinity and molecular interactions of materials. Fig. S2 shows Raman spectra of C-Z-ZnO-rGO nanocomposites. The peaks at 330, 435, 512 and 573 cm^{-1} correspond to Raman-activated $E_{1\ (TO)}$, $E_{2\ (TO)}$, $E_{1(LO)}$, and $A_{1(TO)}$ phonon modes of ZnO, respectively. The vibration modes "TO" and "LO" represent transverse and longitudinal optical phonon mode, respectively. At the same time, the P_1 and P_2 peaks at 728 and 1460 cm^{-1} are attributed to surface defects and phonon restriction effect [3, 4]. The characteristic peaks at 1357 and 1609 cm^{-1} correspond to the D and G peaks of rGO, respectively. The D peak is generated by disordered sp^2 carbon atoms and associated with lattice vibrations away from the center of the Brillouin zone. A weak D peak correspond to low structural defects in the graphene. The G peak is caused by the in-plane vibration of the sp^2 carbon atom of rGO, and its intensity reflect the layer number of graphene. The intensity ratio I_D/I_G is used to define the disorder degree in carbon-based materials [5]. Therefore, Raman results confirm that C-Z-ZnO-rGO nanocomposites are successfully fabricated.

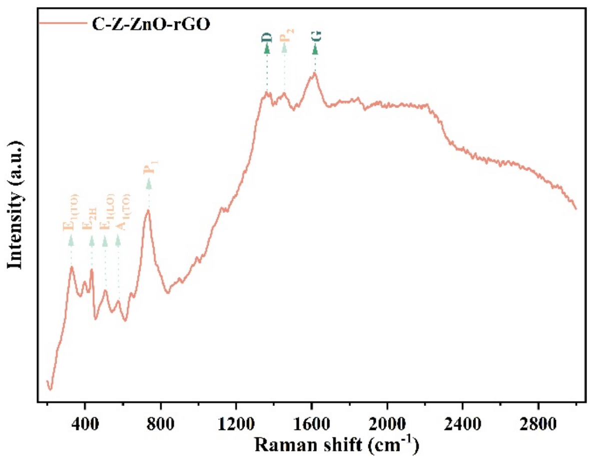

Fig. S2 Raman spectra of C-Z-ZnO-rGO nanocomposites.

The initial resistance value (R_a) of Z-ZnO, C-Z-Z-ZnO and C-Z-ZnO-rGO at different temperatures are shown in Fig. S3. The initial resistance is the average value before injecting the target gas. As the temperature increases, the resistance of semiconductor materials is decreased. The main reason is that the generation and recombination of electron hole pairs will reach dynamic equilibrium at a certain temperature, in this case, the semiconductor has a certain carrier density and resistivity. However, more electron hole pairs will be generated with the increase of the temperature, which cause the carrier density is increased and the resistance value is decreased. Compared with C-Z-ZnO, the change in the initial resistance value of Z-ZnO is small, mainly because the cotton body of C-Z-ZnO cotton is removed after calcination at 500 °C, and only the cotton fiber template is retained. Compared with C-Z-ZnO, the initial resistance value of C-Z-ZnO-rGO is significantly reduced, mainly because the conductivity of C-Z-ZnO is increased with the addition of rGO.

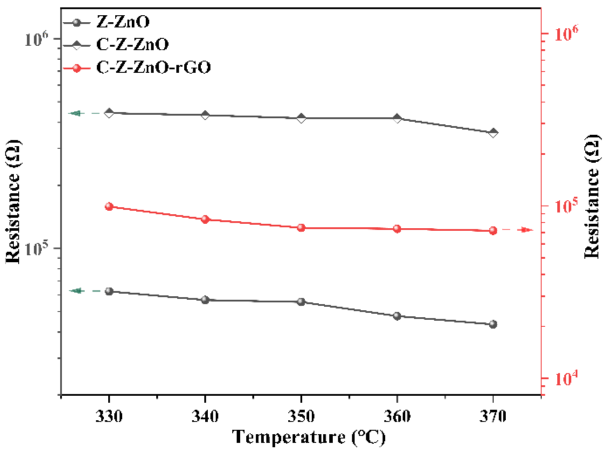

Fig. S3 Resistance (R_a) of Z-ZnO, C-Z-ZnO and C-Z-ZnO-rGO gas sensors in air at different temperatures.

The repeatability of a gas sensor is defined as the response curve remaining essentially unchanged during each successive complete test cycle using the gas sensor at a constant target gas concentration and operating temperature. In this work, Z-ZnO, C-Z-ZnO, and C-Z-ZnO-rGO gas sensors are prepared to verify the repeatability of the gas sensors. Five repeatability tests of the Z-ZnO, C-Z-ZnO and C-Z-ZnO-rGO gas sensor for 100 ppm acetic acid gas are shown in Fig. S4 (a-c). Meanwhile, we compared the gas-sensitive performance and calculate the average values of initial resistance value, response/recovery time and response value of the same gas-sensitive material in five tests, as shown in Table S1.

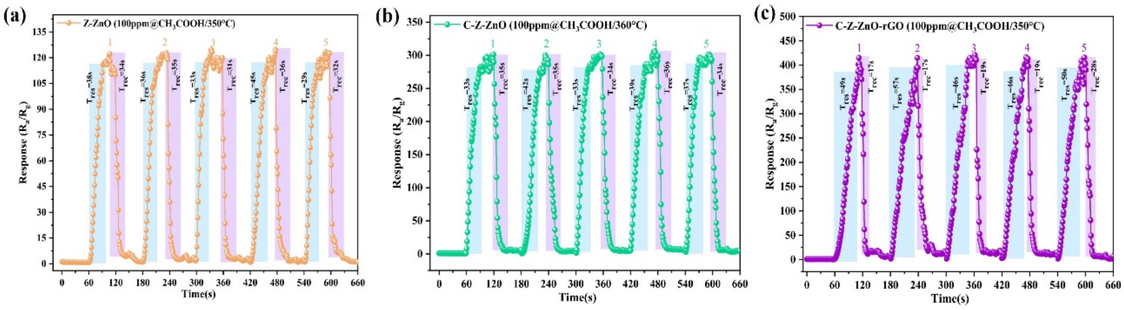

Fig. S4 Response-recovery curves within five cycles of (a) Z-ZnO gas sensor at 350 °C, (b) C-Z-ZnO gas sensor at 360 °C and (c) C-Z-ZnO-rGO gas sensor at 350 °C for 100 ppm acetic acid.

Table S1 Comparison of the initial resistance values, response/recovery time, and response values of Z-ZnO, C-Z-ZnO, C-Z-ZnO-rGO for five cycles testing for 100ppm acetic acid gas at optimal temperature.

Samples	Initial Resistance (Ω)	Response Time(s)	Recovery Time(s)	Response (R_a/R_g)
Z-ZnO-1	52781.463	38	34	122.257
Z-ZnO-2	56321.738	36	35	122.537
Z-ZnO-3	55432.368	33	31	124.585
Z-ZnO-4	58233.718	45	36	124.828
Z-ZnO-5	52704.206	29	32	123.531
Average values	**55094.699**	**36**	**34**	**123.548**
C-Z-ZnO-1	75642.387	33	35	301.266
C-Z-ZnO-2	71583.775	42	35	300.145
C-Z-ZnO-3	73892.863	33	34	301.625
C-Z-ZnO-4	69003.242	39	36	306.558
C-Z-ZnO-5	77275.936	37	34	300.939
Average values	**73479.641**	**37**	**35**	**302.107**

C-Z-ZnO-rGO-1	418359.862	49	17	415.876
C-Z-ZnO-rGO -2	399487.674	57	17	415.983
C-Z-ZnO-rGO -3	435782.342	46	19	420.627
C-Z-ZnO-rGO -4	426093.418	46	19	415.954
C-Z-ZnO-rGO -5	397983.716	50	28	415.526
Average values	**415541.402**	**50**	**20**	**416.793**

References

[1] Q.R. Zeng, J.T. Feng, X.C. Lin, Y. Zhao, H. Liu, S.Z. Wang, Z.J. Dong, W. Feng, J. Alloy. Compd., 2020, **815**, 150550
https://doi.org/10.1016/j.jallcom.2019.05.018

[2] W.H. Li, X.F. Wu, H.D. Liu, J.Y. Chen, W.X. Tang, Y.F. Chen, New J. Chem., 2015, **39**, 7060-7065
https://doi.org/10.1039/C5NJ00549C

[3] M. Sahoo, R. P. Antony, T. Mathews, S. Dash, and A. K. Tyagi, AIP Conf. Proc., 2013, **1512**, 1262.
https://doi.org/10.1063/1.4791511

[4] H.J. Gao, Y.Z. Ma, P. Song, J.F. Leng , Q. Wang, J. Mater. Sci., 2021, **32** 10058-10069.
https://doi.org/10.1007/s10854-021-05664-5

[5] J.J. Ding, H.F. Dai, H.X. Chen, Y.X. Jin , H.W. Fu, B. Xiao, Sens. Actuators B, 2022, **372**, 132655.
https://doi.org/10.1016/j.snb.2022.132655